Research Article | Vol. 25, No. 13 | 26 Jun 2017 | OPTICS EXPRESS 13990
Optics EXPRESS

Vector fields in a tight laser focus: comparison of models

JUSTIN PEATROSS,* MANUEL BERRONDO, DALLAS SMITH, AND MICHAEL WARE

Department of Physics and Astronomy, Brigham Young University, Provo, Utah 84602, USA
*peat@byu.edu

Abstract: We assess several widely used vector models of a Gaussian laser beam in the context of more accurate vector diffraction integration. For the analysis, we present a streamlined derivation of the vector fields of a uniformly polarized beam reflected from an ideal parabolic mirror, both inside and outside of the resulting focus. This exact solution to Maxwell's equations, first developed in 1920 by V. S. Ignatovsky, is highly relevant to high-intensity laser experiments since the boundary conditions at a focusing optic dictate the form of the focus in a manner analogous to a physical experiment. In contrast, many models simply assume a field profile near the focus and develop the surrounding vector fields consistent with Maxwell's equations. In comparing the Ignatovsky result with popular closed-form analytic vector models of a Gaussian beam, we find that the relatively simple model developed by Erikson and Singh in 1994 provides good agreement in the paraxial limit. Models involving a Lax expansion introduce divergences outside of the focus while providing little if any improvement in the focal region. Extremely tight focusing produces a somewhat complicated structure in the focus, and requires the Ignatovsky model for accurate representation.

OCIS codes: (260.1960) Diffraction theory; (140.3295) Laser beam characterization; (260.2110) Electromagnetic optics; (260.5430) Polarization.

References and links

1. M. Lax, W. Louisell, and W. McKnight, "From Maxwell to paraxial wave optics," Phys. Rev. A **11**, 1365–1370 (1975).
2. L. W. Davis, "Theory of electromagnetic beams," Phys. Rev. A **19**, 1177–1179 (1979).
3. Y. Fainman and J. Shamir, "Polarization of nonplanar wave fronts," Appl. Opt. **23**, 3188–3195 (1984).
4. T. Takenaka, M. Yokota, and O. Fukumitsu, "Propagation of light beams beyond the paraxial approximation," J. Opt. Soc. A **2**, 826–829 (1985).
5. J. P. Barton and D. R. Alexander, "Fifth-order corrected electromagnetic field components for a fundamental Gaussian beam," J. Appl. Phys. **66**, 2800–2802 (1989).
6. L. Cicchitelli, H. Hora and R. Postle, "Longitudinal field components for laser beams in vacuum," Phys. Rev. A **41**, 3727–3732 (1990).
7. W. Erikson and S. Singh, "Polarization properties of Maxwell-Gaussian laser beams," Phys. Rev. E **49**, 5778–5786 (1994).
8. P. Varga and P. Török, "The Gaussian wave solution of Maxwell's equations and the validity of scalar wave approximation," Opt. Comm. **152**, 108–118 (1998).
9. H.-C. Kim, Y. H. Lee, "Hermite-Gaussian and Laguerre-Gaussian beams beyond the paraxial approximation," Opt. Comm. **169**, 9–16 (1999).
10. Y. Salamin and C. Keitel, "Electron acceleration by a tightly focused laser beam," Phys. Rev. Lett. **88**, 095005 (2002).
11. S. M. Sepke and D. P. Umstadter, "Exact analytical solution for the vector electromagnetic field of Gaussian, flattened Gaussian, and annular Gaussian laser modes," Opt. Lett. **31**, 1447–1449 (2006).
12. Y. I. Salamin, "Fields of a Gaussian beam beyond the paraxial approximation," Appl. Phys. B **86**, 319–326 (2007).
13. Y. I. Salamin, "Simple analytical derivation of the fields of an ultrashort tightly focused linearly polarized laser pulse," Phys. Rev. A **92**, 063818 (2015).
14. U. Levy and Y. Silberberg, "Weakly diverging to tightly focused Gaussian beams: a single set of analytic expressions," J. Opt. Soc. Am. A **33**, 1999–2009 (2016).
15. V. Yanovsky, V. Chvykov, G. Kalinchenko, P. Rousseau, T. Planchon, T. Matsuoka, A. Maksimchuk, J. Nees, G. Cheriaux, G. Mourou, and K. Krushelnick, "Ultra-high intensity- 300-TW laser at 0.1 Hz repetition rate," Opt. Express **16**, 2109–2114 (2008).
16. G. Mourou, T. Tajima, "More intense, shorter pulses," Science **331**, 41-42 (2011).
17. N.V. Zamfir, "Nuclear Physics with 10PW laser beams at extreme light infrastructure–nuclear physics (ELI-NP)," Eur. Phys. J. Special Topics **223**, 1221-1227 (2014).

#287287 https://doi.org/10.1364/OE.25.013991
Journal © 2017 Received 23 Feb 2017; revised 23 May 2017; accepted 24 May 2017; published 12 Jun 2017

Optics EXPRESS

18. B. Quesnel and P. Mora, "Theory and simulation of the interaction of ultraintense laser pulses with electrons in vacuum," Phys. Rev. E **58**, 3719–3732 (1998).
19. M. Scully and M. Zubairy, "Simple laser accelerator: Optics and particle dynamics," Phys. Rev. A **152**, 108–118 (1998).
20. S. G. Bochkarev, Y. Yu. Bychenkov, "Acceleration of electrons by tightly focused femtosecond laser pulses," Quantum Electron. **37**, 273–284 (2007).
21. K. I. Popov, V. Yu. Bychenkov, W. Rozmus, and R. D. Sydora, "Electron vacuum acceleration by a tightly focused laser pulse," Phys. Plasmas **15**, 013108 (2008).
22. N. Powers, I. Ghebregziabher, G. Golovin, C. Liu, S. Chen, S. Banerjee, J. Zhang and D. Umstadter, "Quasi-monoenergetic and tunable X-rays from a laser-driven Compton light source," Nature Photonics **8**, 28-31 (2014).
23. M. Ware, E. Cunningham, C. Coburn, J. Peatross, "Measured photoemission from electron wave packets in a strong laser field," Opt. Lett. **41**, 689–692 (2016).
24. C.P. Ridgers, J.G. Kirk, R. Duclous, T.G. Blackburn, C.S. Brady, K. Bennette, T.D. Arbere, A.R. Bell, "Modelling gamma-ray photon emission and pair production in high-intensity laser-matter interactions," J. Comput. Phys. **260**, 273–285 (2014).
25. I. Ghebregziabher, B. A. Shadwick, and D. Umstadter, "Spectral bandwidth reduction of Thomson scattered light by pulse chirping," Phys. Rev. Spec. Top. - Accel. Beams **16**, 030705 (2013).
26. G. Pariente, V. Gallet, A. Borot, O. Gobert, and F. Quéré, "Space-time characterization of ultra-intense femtosecond laser beams," Nature Photonics **10**, 547–553 (2016).
27. V. S. Ignatovsky, "The relationship between geometric and wave optics and diffraction of an azimuthally symmetric beam," Trans. Opt. Inst. Petrograd **1**, paper 3 (1920).
28. V. S. Ignatovsky, "Diffraction by a lens with arbitrary aperture," Trans. Opt. Inst. Petrograd **1**, paper 4 (1920).
29. V. S. Ignatovsky, "Diffraction by a parabolic mirror having arbitrary opening," Trans. Opt. Inst. Petrograd **1**, paper 5 (1920).
30. E. Wolf, "Electromagnetic diffraction in optical systems. I. An integral representation of the image field," Proc. R. Soc. A **253**, 349–357 (1959).
31. B. Richards and E. Wolf, "Electromagnetic diffraction in optical systems. II. Structure of the image field in an aplanatic system," Proc. R. Soc. A **253**, 358-379 (1959).
32. A. Yoshida and T. Asakura, "Electromagnetic Field near the focus of Gaussian Beams," Optik **41**, 281–292 (1974).
33. C. J. R. Sheppard, A. Choudhury, and J. Gannaway, "Electromagnetic field near the focus of wide-angular lens and mirror systems," IEEE J. Microwave Opt. Acoust. **1**, 129–132 (1977).
34. R. Barakat, "Diffracted electromagnetic fields in the neighborhood of the focus of a paraboloidal mirror having a central obscuration," Appl. Opt. **26**, 3790–3795 (1987).
35. W. Hsu and R. Barakat, "Stratton-Chu vectorial diffraction of electromagnetic fields by apertures with application to small-Fresnel-number systems," J. Opt. Soc. Am. A **26**, 623–629 (1994).
36. P. Varga and P. Török, "Focusing of electromagnetic waves by paraboloid mirrors. I. Theory," J. Opt. Soc. Am. A **17**, 2081–2089 (2000).
37. M. A. Lieb and A. J. Meixner, "A high numerical aperture parabolic mirror as imaging device for confocal microscopy," Opt. Express **8**, 458–474 (2001).
38. C. J. R. Sheppard, "High-aperture beams," J. Opt. Soc. Am. A **18**, 1579–1587 (2001).
39. N. Bokor, N. Davidson, "4π Focusing with single paraboloid mirror," Opt. Comm. **281**, 5499–5503 (2008).
40. P. Debye, "Das Verhalten von Lichtwellen in der Nähe eines Brennpunktes oder einer Brennlinie," Ann. Phys. **30**, 755–776 (1909).
41. J. D. Jackson, *Classical Electrodynamics*, 3rd ed. (Wiley, 1998), Eq. (10.87).
42. J. A. Stratton and L. J. Chu, "Diffraction Theory of Electromagnetic Waves," Phys. Rev. **56**, 99-107 (1939).
43. S. Bahk, P. Rousseau, T. Planchon, V. Chvykov, G. Kalintchenko, A. Maksimchuk, G. Mourou, and V. Yanovsky, "Generation and characterization of the highest laser intensities (10^{22} W/cm^2)," Opt. Lett. **29**, 2837–2839 (2004).
44. $\int_0^{2\pi} \mathrm{d}\phi' \cos n\phi' e^{\pm ia\cos(\phi'-\phi)} = 2\pi(\pm i)^n \cos n\phi J_n(a)$, $\int_0^{2\pi} \mathrm{d}\phi' \sin n\phi' e^{\pm ia\cos(\phi'-\phi)} = 2\pi(\pm i)^n \sin n\phi J_n(a)$
45. J. J. Stamns, *Waves in Focal Regions*, (IOP Publishing, 1986), Sec. 16.1.
46. R. K. Luneburg, *Mathematical Theory of Optics*, (University of California Press, 1966), Sec. 46.
47. M. Born and E. Wolf, *Principles of Optics*, 7th ed. (Cambridge University Press, 1999), Sec. 8.8.1.
48. Note that $J_n'(x) = \frac{1}{2}[J_{n-1}(x) - J_{n+1}(x)]$ and $2nJ_n(x) = x[J_{n-1}(x) + J_{n+1}(x)]$.
49. H. Luo, S. Liu, Z. Lin, and C. T. Chan, "Method for accurate description of a radially polarized Gaussian laser beam beyond the paraxial approximation," Opt. Lett. **32**, 1692–1694 (2007).
50. M. H. Holmes, *Introduction to Perturbation Methods*, 2nd Ed. (Springer, 2013).
51. C. Sheppard and K. Larkin, "Optimal concentration of electromagnetic radiation," J. Mod. Opt. **41**, 1495–1505 (1994).
52. I. Gonoskov, A. Aiello, S. Heugel, and G. Leuchs, "Dipole pulse theory: Maximizing the field amplitude from 4π focused laser pulses," Phys. Rev. A **86**, 053836 (2012).
53. ru.wikipedia.org, search V. S. Ignatowsky; en.wikipedia.org, search V. S. Ignatowski.
54. $\int_{-\infty}^{\infty} \mathrm{d}u\, e^{iau^2} = (1+i)\sqrt{\frac{\pi}{2a}}$

Optics EXPRESS

1. Introduction

The laser community has worked to effectively model vector fields in a tightly focused laser for several decades. Rigorous vector diffraction integrals typically require numerical evaluation, so for many applications researchers prefer an approximate model that is analytic. A variety of models have been proposed, which often differ markedly from each other [1–14]. These differences are of concern to anyone who uses computational models to study interactions in the laser focus. However, comparisons between vector focal models are conspicuously absent in the literature. Clarification and arbitration between the various approaches is needed, which is the aim of this article.

We compare several of the most common approaches to modeling vector fields in a focus. We show that in the paraxial limit, the closed-form analytic model developed by Erikson and Singh [7] closely resembles rigorous diffraction theory applied to a Gaussian beam reflected from a parabolic mirror. In contrast with other models, the Singh model imitates the beam well in both the near and far field. The closed-form formula by Barton and Alexander [5] gives marginal improvement in the focal region at the expense of divergences outside the focus. For lower f-numbers, the full integral formula by Ignatovsky is needed for accurate results.

We find that a primary reason for the discrepancies between models is that many models start from an *assumed* field profile in the focus and then develop vector fields in the surrounding region, consistent with Maxwell's equations. We demonstrate that typical assumed starting points are often inconsistent with the experimentally relevant boundary condition imposed by a collimated beam incident on a focusing optic. We thus assert that the boundary condition at the focusing optic is of paramount concern in all practical experimental situations.

This analysis and comparison of various vector focal models is of particular relevance to the high-intensity laser community, which expends significant effort to achieve the highest possible laser intensities. High-end laser systems can currently achieve intensities around 10^{22} W/cm^2 using tight focusing, and many groups continue to work to attain intensities beyond this level [15–17]. These extreme intensities open new research possibilities, such as particle acceleration [18–23], gamma-ray and electron-positron-pair production [24,25] as well as nuclear interactions [17]. To model such phenomena, an accurate accounting of the electric and magnetic vector field distribution throughout a tight focus is often critical [26].

Rigorous vector diffraction theory of focused light [27–39] has been developed over the course of nearly a century, beginning with a treatment in 1920 by V. S. Ignatovsky [27–29]. Ignatovsky first made the key realization that the optical elements used to focus the light, such as mirrors and lenses, dictate a boundary condition on the vector components of the converging field. Ignatovsky developed vector diffraction for a uniformly polarized collimated beam reflected from a parabolic mirror [29]. At the curved mirror surface, the vector field components are modified by the act of reflection as a function of position. Ignatovsky also worked out the vector field components of a polarized beam traversing a lens [28]. The specifics of the focusing optic give rise to different spatial amplitude distributions, referred to as apodizing functions, for the individual vector field components.

Ignatovsky's approach is related to the work of Debye, who in 1909 showed how to invert the traditional diffraction problem. Rather than starting in a focal plane (or at a confining aperture) and working outward, Debye computed the fields in a focus starting from a converging spherical wave [40]. Ignatovsky recognized the practical relevance of this approach since the experimenter has control over (or at least access to the characterization of) the field distribution of the beam incident on the focusing optic, which endows the field distribution with the characteristics that appear in the focus.

The Ignatovsky formulation is an exact solution to Maxwell's equations consistent with the experimentally relevant boundary condition. It provides a 'gold standard' with which to evaluate the performance of the various simpler analytic models offered in the literature. In this

Optics EXPRESS

paper, we first outline the rigorous diffraction integrals that generate vector fields in the focus arising from a collimated beam incident on an idealized parabolic mirror. Our derivation of the Ignatovsky's diffraction formula is simplified and streamlined relative to earlier treatments. We point out that there is no need to transfer the incident field onto a converging spherical surface before performing the diffraction integral, which shortens the development. With the Ignatovsky formulation in hand, we then compare and contrast its results with other models from the literature.

2. Reflection from a parabolic mirror

The vector diffraction theory developed here can be applied to both lenses and mirrors with a large range of prescriptions. We specialize our analysis to the focusing of a linearly-polarized collimated beam by a parabolic mirror, since the high-intensity community employs this focusing scheme most commonly. The results discussed here differ in detail from other focusing optics.

The first step is to write the fields arising from a collimated beam just after reflection from a parabolic mirror. In his original derivation, Ignatovsky employed parabolic coordinates, but we elect to use cartesian coordinates. We consider an ideal parabolic mirror of focal length f oriented with its axis of symmetry along the z axis and situated so that its surface intersects the z-axis a distance f to the left of the origin, as shown in Fig. 1. We denote the mirror surface using primed coordinates as

$$z' = -f + \frac{\rho'^2}{4f} \quad \text{and} \quad \rho' = \sqrt{x'^2 + y'^2}. \tag{1}$$

The surface normal is then given by

$$\hat{\mathbf{n}}(x', y') = \frac{-\frac{1}{2f}\,(x'\hat{\mathbf{x}} + y'\hat{\mathbf{y}}) + \hat{\mathbf{z}}}{\sqrt{1 + \frac{\rho'^2}{4f^2}}}, \tag{2}$$

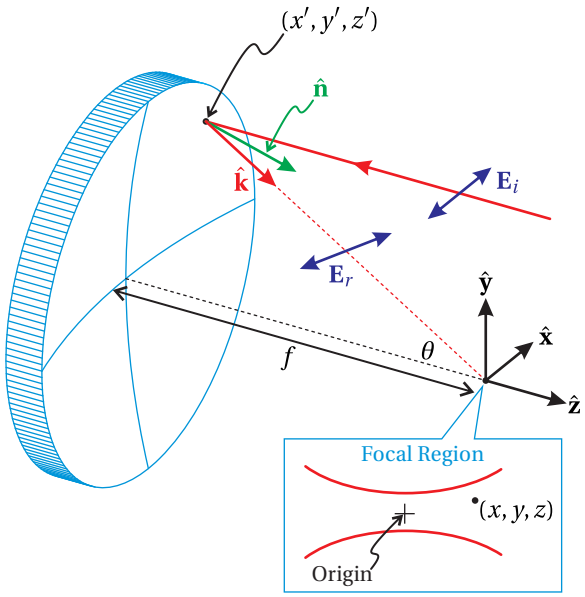

Fig. 1. Incident light (x-polarized) reflected by a parabolic mirror. s- and p-polarized components of the field reflect as plane waves about the local surface normal $\hat{\mathbf{n}}$.

Optics EXPRESS

Note that $x'\hat{\mathbf{x}} + y'\hat{\mathbf{y}} = \rho'\hat{\boldsymbol{\rho}}'$, where $\hat{\boldsymbol{\rho}}'$ is the radial unit vector.

We define the incident field at the mirror surface to be an x-polarized plane wave, traveling in the $-\hat{\mathbf{z}}$ direction and multiplied by a smoothly-varying lateral envelope, given by

$$\mathbf{E}_{\mathrm{i}}(x', y') = \hat{\mathbf{x}} E_{\mathrm{env}}(x', y') e^{i\left(-k(z'+f)-\omega t\right)}. \tag{3}$$

The phase of the envelope $E_{\mathrm{env}}(x', y')$ is referenced to the center of the mirror surface, $\rho' = 0$ and $z' = -f$. In vacuum, the wavenumber is related to the frequency by $k = \omega/c$. We permit only slow transverse variations in the envelope $E_{\mathrm{env}}(x', y')$. The incident beam width and mirror dimension are assumed to be enormous compared to a wavelength. These requirements allow us to treat the local incident and reflected fields as plane-wave like at a given point on the mirror. For purposes of reflection, the local p-polarized component of the incident field lies along $\hat{\boldsymbol{\rho}}' = (x'\hat{\mathbf{x}} + y'\hat{\mathbf{y}})/\rho'$ with strength $E_{\mathrm{env}}(x', y')x'/\rho'$. The local s-polarized component of the incident field lies along $\hat{\mathbf{s}} = (-y'\hat{\mathbf{x}} + x'\hat{\mathbf{y}})/\rho'$ with strength $-E_{\mathrm{env}}(x', y')y'/\rho'$.

We make the idealized assumption that the amplitude and phase change of the fields upon reflection is uniform over the mirror surface, and omit any overall phase factor. After reflection about the surface normal $\hat{\mathbf{n}}$, the local fields travel toward the focus (i.e. the origin) along the direction

$$\hat{\mathbf{k}}(x', y') = \frac{-\frac{1}{f}(x'\hat{\mathbf{x}} + y'\hat{\mathbf{y}}) + \left(1 - \frac{\rho'^2}{4f^2}\right)\hat{\mathbf{z}}}{1 + \frac{\rho'^2}{4f^2}}. \tag{4}$$

The orientation of the local s-polarized field remains unchanged, but the new p-polarized field component aligns along $\hat{\mathbf{s}} \times \hat{\mathbf{k}}$.

Combining the reflected s- and p-polarized field components, we obtain the following unit vector representing the local direction of electric-field polarization after reflection:

$$\hat{\mathbf{p}}^{(E)}(x', y') = \frac{\left(1 - \frac{x'^2 - y'^2}{4f^2}\right)\hat{\mathbf{x}} - \frac{x'y'}{2f^2}\hat{\mathbf{y}} + \frac{x'}{f}\hat{\mathbf{z}}}{1 + \frac{\rho'^2}{4f^2}} \tag{5}$$

The reflected field at the surface defined by (1) is then

$$\mathbf{E}^{(r)}_{\mathrm{surface}}(x', y') = \hat{\mathbf{p}}^{(E)}(x', y')\, E_{\mathrm{env}}(x', y')\, e^{i\left(-\frac{k\rho'^2}{4f} - \omega t\right)} \tag{6}$$

This field locally propagates in direction $\hat{\mathbf{k}}$ (not explicitly expressed in (6) since the field has been evaluated on the parabolic surface).

The associated magnetic field at the surface is

$$\mathbf{B}^{(r)}_{\mathrm{surface}}(x', y') = \hat{\mathbf{p}}^{(B)}(x', y')\, \frac{E_{\mathrm{env}}(x', y')}{c} e^{i\left(-\frac{k\rho'^2}{4f} - \omega t\right)} \tag{7}$$

where $\hat{\mathbf{p}}^{(B)}$ is a rotated version of $\hat{\mathbf{p}}^{(E)}$ obtained from the transform $x' \to y'$ and $y' \to -x'$ together with the assignments $p_x^{(B)} = -p_y^{(E)}$, $p_y^{(B)} = p_x^{(E)}$, and $p_z^{(B)} = p_z^{(E)}$. Explicitly, the unit vector for the magnetic-field polarization is

$$\hat{\mathbf{p}}^{(B)}(x', y') = \frac{-\frac{x'y'}{2f^2}\hat{\mathbf{x}} + \left(1 + \frac{x'^2 - y'^2}{4f^2}\right)\hat{\mathbf{y}} + \frac{y'}{f}\hat{\mathbf{z}}}{1 + \frac{\rho'^2}{4f^2}} \tag{8}$$

Importantly, the polarization unit vectors Eqs. (5) and (8), which we shall call Ignatovsky vectors, obey the rules

$$\hat{\mathbf{p}}^{(E)} \times \hat{\mathbf{p}}^{(B)} = \hat{\mathbf{k}}, \quad \hat{\mathbf{k}} \cdot \hat{\mathbf{p}}^{(E)} = 0, \quad \text{and} \quad \hat{\mathbf{k}} \cdot \hat{\mathbf{p}}^{(B)} = 0. \tag{9}$$

Figure 2 plots the fields in (6) and (7) for the case of a Gaussian field envelope.

Optics EXPRESS

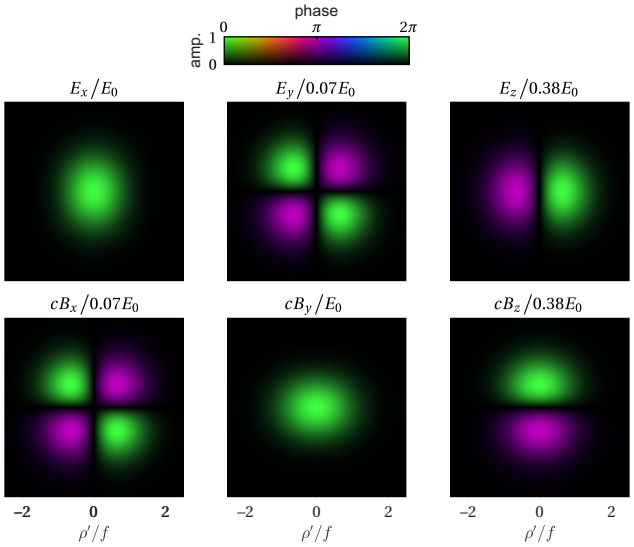

Fig. 2. Field components for a Gaussian-envelope beam with $E_{\text{env}}(x', y') = E_0 e^{-\rho'^2/w^2}$, immediately after reflection from a parabolic mirror. The fields are computed for $f/(2w) = 0.5$ ($NA = 0.8$) on the surface of the mirror as a function of x' and y' (horizontal and vertical in the figure). The rapidly-varying phase factors in (6) and (7) are removed for clarity. Each box has dimensions $4f \times 4f$, where f is the focal length of the mirror.

3. Green's theorem and the Debye limit

Now that we have a representation of the fields just after reflection, our next task is to produce the fields downstream from the mirror. We consider a single-frequency solution to Maxwell's equations, which obeys the Helmholtz equation. Green's theorem applied to the electric field may be written as [41]

$$\mathbf{E}(x, y, z) = \oint_{S'} dA' [\mathbf{E}^{(r)}(\hat{\mathbf{n}} \cdot \nabla' G) - G(\hat{\mathbf{n}} \cdot \nabla')\mathbf{E}^{(r)}] \tag{10}$$

where $G = e^{ikR}/(4\pi R)$ and

$$R = |\mathbf{r} - \mathbf{r}'| = r' \sqrt{1 - 2\frac{\mathbf{r}' \cdot \mathbf{r}}{r'^2} + \frac{r^2}{r'^2}} \to r' - \frac{\mathbf{r}' \cdot \mathbf{r}}{r'}, \tag{11}$$

with $\mathbf{r}' = x'\hat{\mathbf{x}} + y'\hat{\mathbf{y}} + z'\hat{\mathbf{z}}$ and $\mathbf{r} = x\hat{\mathbf{x}} + y\hat{\mathbf{y}} + z\hat{\mathbf{z}}$.

The final form of (11) is known as the Debye limit, which retains full consistency with Maxwell's equations when used in the exponent of G, as will be later pointed out. The only assumption is that the mirror resides far from the focus. In the truncated Taylor-series expansion of the square root, the term r^2/r'^2 is neglected under the assumption that x, y, and z lie in the neighborhood of the focus (origin). In the denominator of G, we represent R simply by r'. Remarkably, there will be no residual restriction on the values for x, y, or z, as will be pointed out later. On the parabolic surface, when z' is replaced by (1), we have $\mathbf{r}' = -r'\hat{\mathbf{k}}(x', y')$ and $r' = f + \frac{\rho'^2}{4f}$.

To summarize, (10) indicates that, in the absence of sources or sinks, the vector field at point x, y, z inside a volume can be determined entirely from the fields at surface S' bounding that volume. We denote points on this bounding surface with x', y', z'. The entire surface S' is comprised of the mirror surface and a large secondary surface that extends beyond the point

Optics EXPRESS

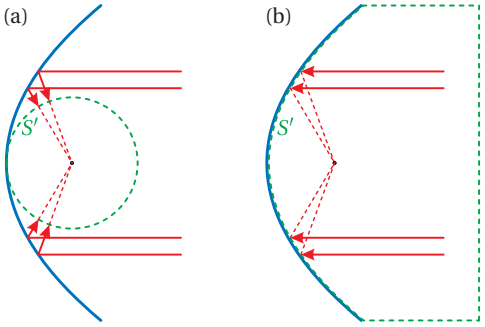

Fig. 3. (a) Transfer of fields onto a spherical surface prior to diffraction calculation. (b) Direct use of fields at parabolic surface in diffraction calculation.

x, y, z to enclose a volume as shown in Fig. 3(b). However, the secondary surface with its exiting flux contributes nothing (on average) to the integral and may safely be ignored. We include only light that has reflected exactly once from the parabolic surface in the problem; the collimated beam incident on the parabola and secondary reflections are treated external to the problem. Note that (10) applies equally well to the magnetic field; simply trade **B** for **E**.

In previous derivations, including the original one by Ignatovsky, geometrical optics was first used to propagate the field from the parabolic mirror to a spherical surface that touches the mirror in the center, as shown in Fig. 3(a). The diffraction integral was then performed over the spherical surface. This intermediate propagation is an unnecessary step, since it is straight forward to perform the diffraction integral over the parabolic surface, as in Fig. 3(b).

Some authors [33] have employed the Stratton-Chu formulation [42] of Green's theorem (involving both the electric and magnetic field after substitutions from Maxwell's equations). This approach is designed to deal with cropping of the incident field by an sharp aperture, resulting in an added contour integral around the aperture. Our assumption that the field varies only gradually in the lateral dimension precludes the use of a sharp aperture, which is a rare situation in high-intensity laser physics.

4. Ignatovsky diffraction

There remains the task of computing the spatial derivatives in (10). Recall that (6) is the amplitude of a plane-wave-like field that locally propagates in the $\hat{\mathbf{k}}$ direction, with the assumption that $E_{\text{env}}(x', y')$ varies slowly laterally at the mirror. This implies that $(\hat{\mathbf{n}} \cdot \nabla')\mathbf{E}^{(r)} \to ik(\hat{\mathbf{n}} \cdot \hat{\mathbf{k}})\mathbf{E}^{(r)}$. In the same spirit, we also have $\nabla' G \to -ik\hat{\mathbf{k}}G$. The paraboloid area element may be written as $dA' = dx'dy'/(\hat{\mathbf{n}} \cdot \hat{\mathbf{z}})$, where $\hat{\mathbf{n}} \cdot \hat{\mathbf{z}}$ is the cosine of the angle between the parabolic surface and the x-y plane.

With these preliminaries, Green's theorem applied to (6) produces

$$\mathbf{E}(x, y, z) = -i\frac{ke^{i(kf-\omega t)}}{2\pi f}\int_{-\infty}^{\infty}\int_{-\infty}^{\infty}\frac{dx'dy'}{1+\frac{\rho'^2}{4f^2}}E_{\text{env}}(x', y')\,\hat{\mathbf{p}}^{(E)}(x', y')\,e^{ik\hat{\mathbf{k}}(x',y')\cdot\mathbf{r}} \quad (12)$$

This formula may be applied to any (smooth) field distribution incident on the parabola, including an off-axis incident beam such as considered in Ref. [43]. Similarly, the corresponding magnetic field is

$$\mathbf{B}(x, y, z) = -i\frac{ke^{i(kf-\omega t)}}{2\pi f}\int_{-\infty}^{\infty}\int_{-\infty}^{\infty}\frac{dx'dy'}{1+\frac{\rho'^2}{4f^2}}\frac{E_{\text{env}}(x', y')}{c}\hat{\mathbf{p}}^{(B)}(x', y')\,e^{ik\hat{\mathbf{k}}(x',y')\cdot\mathbf{r}} \quad (13)$$

Optics EXPRESS

If the distribution $E_{\text{env}}(x', y')$ is centered on the paraboloid axis and depends only on radius, for example a Gaussian beam with $E_{\text{env}}(\rho') = E_0 e^{-\rho'^2/w^2}$, it becomes convenient to change to cylindrical coordinates: $x = \rho\cos\phi$, $y = \rho\sin\phi$, $x' = \rho'\cos\phi'$, $y' = \rho'\sin\phi'$ with

$$\int_{-\infty}^{\infty}\int_{-\infty}^{\infty} dx'dy' \rightarrow \int_0^{\infty} \rho' d\rho' \int_0^{2\pi} d\phi'. \tag{14}$$

Then $x'^2 - y'^2 = \rho'^2\cos 2\phi'$, $2x'y' = \rho'^2\sin 2\phi'$, and $xx' + yy' = \rho'\rho\cos(\phi - \phi')$. In this case, the azimuthal integration can be performed [44], and (12) simplifies to [29, 33, 34, 37, 45]

$$\mathbf{E}(x, y, z) = -ikfe^{i(kf-\omega t)}\left[\hat{\mathbf{x}}\left(I_0 + \frac{x^2 - y^2}{\rho^2}I_2\right) + \hat{\mathbf{y}}\frac{2xy}{\rho^2}I_2 - i\hat{\mathbf{z}}\frac{x}{\rho}I_1\right] \tag{15}$$

where $\rho = \sqrt{x^2 + y^2}$. We have again favored cartesian variables using $\cos 2\phi = (x^2 - y^2)/\rho^2$, $\sin 2\phi = 2xy/\rho^2$, and $\cos\phi = x/\rho$, which are all finite when $\rho = 0$. The solution (15) is in terms of the following 1-D integrals:

$$\begin{aligned} I_0 &= \int_0^{\pi} d\theta E_{\text{e}}(\rho') J_0(k\rho\sin\theta)\sin\theta e^{ikz\cos\theta} \\ I_1 &= 2\int_0^{\pi} d\theta E_{\text{e}}(\rho')\sqrt{\xi(\theta)}J_1(k\rho\sin\theta)\sin\theta e^{ikz\cos\theta} \\ I_2 &= \int_0^{\pi} d\theta E_{\text{e}}(\rho')\xi(\theta)J_2(k\rho\sin\theta)\sin\theta e^{ikz\cos\theta} \end{aligned} \tag{16}$$

where $\xi(\theta) = (1 - \cos\theta)/(1 + \cos\theta)$ and $\rho'(\theta) = 2f\sqrt{\xi(\theta)}$. To arrive at (16), we introduced a change of integration variable such that $\cos\theta = (1 - \frac{\rho'^2}{4f^2})/(1 + \frac{\rho'^2}{4f^2})$. In this representation, θ may be interpreted as the angle between $\hat{\mathbf{k}}$ and the z-axis, as the integration moves across the mirror surface. The numeric aperture is described by $NA = \sin\theta_0$, where θ_0 is a characteristic angular half width of the converging beam.

Equations (15) and (16) were first derived by Ignatovsky in 1920, following a somewhat cumbersome analysis. For completeness, the magnetic field is given by

$$\mathbf{B}(x, y, z) = -i\frac{kf}{c}e^{i(kf-\omega t)}\left[\hat{\mathbf{x}}\frac{2xy}{\rho^2}I_2 + \hat{\mathbf{y}}\left(I_0 - \frac{x^2 - y^2}{\rho^2}I_2\right) - i\hat{\mathbf{z}}\frac{y}{\rho}I_1\right] \tag{17}$$

Figure 4 plots the electric and magnetic fields in the focal plane $z = 0$ computed via (15) and (17) from the mirror fields depicted Fig. 2. Note the development of diffraction rings surrounding the main beam as the beam propagates from the mirror to the focus.

Equations (15) and (17) may be evaluated to find the fields anywhere in and outside of the focus. In the vicinity of a tight focus, the 1-D integrals (16) are only moderately oscillatory and can be performed rapidly numerically. The numerics depend only on the angular extent of the focusing beam as opposed to its actual distance and physical size, in contrast with other approaches [21]. The formula is exact provided the mirror resides at infinity.

It is straightforward to show that Eqs. (12) and (13) as well as Eqs. (15) and (17) satisfy Maxwell's equations *exactly*. This is not surprising since (12) is recognized merely as a linear superposition of plane waves [46, 47], which obey the properties in (9). The same check can be made on the azimuthally symmetric forms, Eqs. (15) and (17) [48]. A nice feature is that these formulas may be evaluated even *at the mirror*. Appendix A demonstrates that (12) recovers the initial field distribution when evaluated on the mirror surface, provided the mirror is sufficiently far away.

Optics EXPRESS

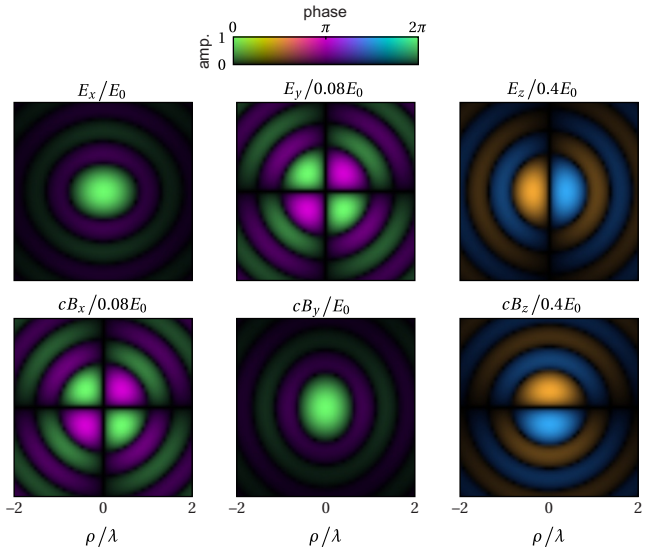

Fig. 4. Field components at $z = 0$ for the Gaussian beam from Fig. 2 focused with $f/(2w) = 0.5$ ($NA = 0.8$). The fields are computed in the plane $z = 0$. Each box has dimensions $4\lambda \times 4\lambda$, where $\lambda = 2\pi/k$, and E_0 denotes the maximum value of E_x.

Since the formula matches the boundary condition at the mirror and obeys Maxwell's equations exactly, Ignatovsky's formula indisputably describes *the* field produced when a linearly polarized collimated beam reflects on axis from an ideal parabolic mirror. Of course, other uniform polarization states can be considered by superimposing (with appropriate phase) a similar solution initially polarized along the y direction. We do not address nonuniform polarization states such as radially [37] or azimuthally polarized beams.

5. Analytic paraxial models

For applications such as simulating laser-matter interactions in an intense tightly focused beam, ideally one would have available a closed analytic formula that adequately represents the field vector components. In this case, one could avoid evaluating the integrals in (16) at each location within the interaction region. The success of paraxial scalar diffraction theory has inspired efforts to formulate corresponding vector-field representations.

For a monochromatic beam, the individual field components obey the Scalar Helmholtz equation: $\nabla^2 U + k^2 U = 0$, where U stands for E_x, E_y, E_z, B_x, B_y, or B_z. If we are interested in a beam-like solution that travels in the z direction, we are encouraged to write $U = U_0 \psi(x, y, z) e^{i(kz-\omega t)}$, whereupon the Helmholtz equation becomes

$$\left(\frac{\partial^2}{\partial x^2} + \frac{\partial^2}{\partial y^2} + \cancel{\frac{\partial^2}{\partial z^2}} + 2ik \frac{\partial}{\partial z} \right) \psi = 0 \tag{18}$$

In the paraxial limit, the second derivative on z may be neglected, and the well-known lowest-order-mode Gaussian-beam solution is then

$$\psi^{(0)} = \frac{z_0}{\mathbb{Z}} \exp\left(-\frac{k}{2} \frac{\rho^2}{\mathbb{Z}} \right), \tag{19}$$

where $\mathbb{Z} = z_0 + iz$, $\rho^2 = x^2 + y^2$, and the Rayleigh range is $z_0 = kw_0^2/2$. One might choose to set $E_x = U$, but care must be taken to find associated field components such that Maxwell's

Optics EXPRESS

equations are satisfied. By direct substitution into Maxwell's equations, Erikson and Singh [7] found corresponding functions for E_y, E_z, B_x, B_y, and B_z to an accuracy commensurate with the paraxial approximation. Their fields for the lowest-order Gaussian mode are

$$\mathbf{E}_{\text{Singh}} = E_0 \left[\hat{\mathbf{x}} + \frac{xy}{2\mathbb{Z}^2}\hat{\mathbf{y}} - i\frac{x}{\mathbb{Z}}\hat{\mathbf{z}}\right]\psi^{(0)}e^{i(kz-\omega t)} \tag{20}$$

$$\mathbf{B}_{\text{Singh}} = \frac{E_0}{c}\left[\frac{xy}{2\mathbb{Z}^2}\hat{\mathbf{x}} + \hat{\mathbf{y}} - i\frac{y}{\mathbb{Z}}\hat{\mathbf{z}}\right]\psi^{(0)}e^{i(kz-\omega t)} \tag{21}$$

They also found vector representations for all paraxial higher-order modes.

Alternatively, one can work with the vector potential $\mathbf{A}$ whose components also obey the scalar Helmholtz equation. Consistent with the Lorenz gauge, Maxwell-respecting fields can be obtained from $\mathbf{B} = \nabla \times \mathbf{A}$ and $\mathbf{E} = ic\nabla(\nabla \cdot \mathbf{A})/k + ick\mathbf{A}$. Conveniently, one may choose $A_y = 0$, $A_z = 0$, and $A_x = A_0\psi e^{i(kz-\omega t)}$ and obtain a Maxwell-respecting field (within the paraxial limit). In this case $B_x = 0$, while in general $E_x, E_y, E_z \neq 0$. We will comment on this asymmetry between the E-field and B-field in the next section.

Lax et al. [1] proposed an iterative scheme whereby an initially paraxial scalar solution could be refined in an effort to accommodate tighter focusing geometries. In this case, (18) is written as

$$\left(\frac{\partial^2}{\partial x^2} + \frac{\partial^2}{\partial y^2} + 2ik\frac{\partial}{\partial z}\right)\psi_{\text{revised}} = -\frac{\partial^2 \psi_{\text{trial}}}{\partial z^2} \tag{22}$$

The paraxial solution (19) fulfills (22) when $\psi_{\text{trial}} = 0$. Davis [2] worked out an analytic expression for the first correction (when ψ_{trial} is set to (19)), Barton and Alexander [5] the second, and Salamin [10] higher-order corrections. After one iterative refinement on $\mathbf{A}_x$, the electric and magnetic fields work out to be

$$\mathbf{E}_{\text{Davis}} = E_0\left[\left(1 + \frac{x^2}{\mathbb{Z}^2} - \frac{k\rho^4}{8\mathbb{Z}^3}\right)\hat{\mathbf{x}} + \frac{xy}{\mathbb{Z}^2}\hat{\mathbf{y}} - i\left(\frac{x}{\mathbb{Z}} - \frac{x}{k\mathbb{Z}^2} + \frac{x\rho^2}{\mathbb{Z}^3} - \frac{kx\rho^4}{8\mathbb{Z}^4}\right)\hat{\mathbf{z}}\right]\psi^{(0)}e^{i(kz-\omega t)} \tag{23}$$

$$\mathbf{B}_{\text{Davis}} = \frac{E_0}{c}\left[\left(1 + \frac{\rho^2}{2\mathbb{Z}^2} - \frac{k\rho^4}{8\mathbb{Z}^3}\right)\hat{\mathbf{y}} - i\left(\frac{y}{\mathbb{Z}} + \frac{y}{k\mathbb{Z}^2} + \frac{y\rho^2}{2\mathbb{Z}^3} - \frac{ky\rho^4}{8\mathbb{Z}^4}\right)\hat{\mathbf{z}}\right]\psi^{(0)}e^{i(kz-\omega t)} \tag{24}$$

It is natural to compare this field distribution with Ignatovsky diffraction both within and outside of the focus. Unfortunately, in all orders of the Lax expansion there appear terms that diverge in the far field. The diverging terms are those with k in the numerator. For example, the x-component of (23) in the far field becomes $E_x \to E_0[1 - \rho^2/z^2 - ik\rho^4/8z^3]$. Note the problematic scaling of the last term with distance z: The *angular* beam width (as well as the beam power) continually grows with distance [14], making any comparison with the far-field meaningless. One cannot, for example, compare the fields at the mirror surface, the starting point for Ignatovsky diffraction. This divergence, first noticed in 2007 [49], calls into question any program based on the Lax iterative scheme. The paraxial solution (19), which seeds the iteration, is valid everywhere; why then should the Lax expansion be trusted in the focal region if it fails in the far field? Nevertheless, as we shall see, these refinements can modestly improve agreement with Ignatovsky diffraction within the focal region.

The divergent behavior of the Lax expansion can be understood in the following context: The paraxial approximation neglects the right-hand term in (22), which corresponds to the highest-order derivative term in z. This changes the structure from an elliptic differential equation to a parabolic differential equation. Furthermore, the number of required boundary conditions goes from two to one. Hence, any further iteration of (22) will yield a singular perturbation expansion [50].

Optics EXPRESS

6. Symmetry considerations

As was pointed out by Barton and Alexander [5], setting $A_y = 0$, $A_z = 0$, and $A_x = A_0\psi e^{i(kz-\omega t)}$ leads to an asymmetry between the E and B fields, as manifest by the lack of an x component in (24). They produced two additional fields from Eqs. (23) and (24) via the assignments

$$\begin{aligned}\mathbf{E}'(x,y)/c &= \hat{\mathbf{x}}B_y(-y,x) - \hat{\mathbf{y}}B_x(-y,x) + \hat{\mathbf{z}}B_z(-y,x)\\ c\mathbf{B}'(x,y) &= -\hat{\mathbf{x}}E_y(y,-x) + \hat{\mathbf{y}}E_x(y,-x) + \hat{\mathbf{z}}E_z(y,-x)\end{aligned} \tag{25}$$

These fields were then averaged with the originals to produce fields that posses the symmetry outlined in connection with (8). To the same order as the Davis model, the Barton model gives

$$\begin{aligned}\mathbf{E}_{\text{Barton}} = E_0\Bigg[&\left(1+\frac{\rho^2+2x^2}{4\mathbb{Z}^2}-\frac{k\rho^4}{8\mathbb{Z}^3}+\alpha_x\right)\hat{\mathbf{x}}+\left(\frac{xy}{2\mathbb{Z}^2}+\alpha_y\right)\hat{\mathbf{y}}\\ &-i\left(\frac{x}{\mathbb{Z}}+\frac{3x\rho^2}{4\mathbb{Z}^3}-\frac{kx\rho^4}{8\mathbb{Z}^4}+\alpha_z\right)\hat{\mathbf{z}}\Bigg]\psi^{(0)}e^{i(kz-\omega t)}\end{aligned} \tag{26}$$

$$\begin{aligned}\mathbf{B}_{\text{Barton}} = \frac{E_0}{c}\Bigg[&\left(\frac{xy}{2\mathbb{Z}^2}+\beta_x\right)\hat{\mathbf{x}}+\left(1+\frac{\rho^2+2y^2}{4\mathbb{Z}^2}-\frac{k\rho^4}{8\mathbb{Z}^3}+\beta_y\right)\hat{\mathbf{y}}\\ &-i\left(\frac{y}{\mathbb{Z}}+\frac{3y\rho^2}{4\mathbb{Z}^3}-\frac{ky\rho^4}{8\mathbb{Z}^4}+\beta_z\right)\hat{\mathbf{z}}\Bigg]\psi^{(0)}e^{i(kz-\omega t)}\end{aligned} \tag{27}$$

The terms $\alpha_x, \alpha_y, \alpha_z, \beta_x, \beta_y, \beta_z$ represent second-order refinements worked out by Barton and Alexander:

$$\begin{aligned}\alpha_x &= \frac{\rho^4+4x^2\rho^2}{8\mathbb{Z}^4}-\frac{3k\rho^6+2kx^2\rho^4}{32\mathbb{Z}^5}+\frac{k^2\rho^8}{128\mathbb{Z}^6}\\ \alpha_y &= \frac{xy\rho^2}{2\mathbb{Z}^4}-\frac{kxy\rho^6}{16\mathbb{Z}^5}\\ \alpha_z &= \frac{5x\rho^4}{8\mathbb{Z}^5}-\frac{5kx\rho^6}{32\mathbb{Z}^6}+\frac{k^2x\rho^8}{128\mathbb{Z}^7}\\ \beta_x &= \alpha_y\\ \beta_y &= \frac{\rho^4+4y^2\rho^2}{8\mathbb{Z}^4}-\frac{3k\rho^6+2ky^2\rho^4}{32\mathbb{Z}^5}+\frac{k^2\rho^8}{128\mathbb{Z}^6}\\ \beta_z &= \frac{5y\rho^4}{8\mathbb{Z}^5}-\frac{5ky\rho^6}{32\mathbb{Z}^6}+\frac{k^2y\rho^8}{128\mathbb{Z}^7}\end{aligned} \tag{28}$$

The terms with k in the numerator diverge in the far field.

Interestingly, the symmetrizing procedure cuts the strength of the y-component of the electric field by a factor of two (and its power by four times). Note the leading terms in the formula by Barton and Alexander agree with the model of Erikson and Singh, Eqs. (20) and (21). In contrast, solutions lacking symmetry such as Eqs. (23) and (24) disagree with Eqs. (20) and (21) and, as we shall see, with the Ignatovsky result also. The divergence issues associated with the Lax expansion are not mitigated by the symmetrization procedure.

The far-field radiation pattern of an electric dipole (near the equator) shares the asymmetric field-component ratios exhibited by Eqs. (23) and (24) to leading order, where the relative strength of the E_y is double that of (20). By superimposing the emission of an oscillating electric dipole and an orthogonal oscillating magnetic dipole, one obtains (to leading order) the symmetry of Eqs. (20) and (21) [51]. Gonoskov and coworkers [52] examined the collimated beam obtained when placing a radiating dipole at the focus of a parabolic mirror. They suggested that if such a beam could be imitated and then focused by a parabolic mirror, one could obtain a sharper focus.

Optics EXPRESS

7. Comparisons

To allow for visual comparison of the different models discussed above, we provide animations showing electric field components for a focused x-polarized Gaussian beam according to the various model. Figure 5 shows an animation for the Ignatovsky model. The top three cells plot E_x, E_y, and E_z in an x-y plane with fixed z. The local phase of the field is indicated by color, while the amplitude is indicated by the brightness of the color. The three lower frames plot the absolute values of these fields along the dashed lines shown in the top three cells. As the animation progresses, z is varied from zero to 100λ, where $\lambda = 2\pi/k$, in an accelerated manner so that the steps in z increase while approaching the far field. The axes for each component are continuously re-scaled to a maximum amplitude of one, with the scaling indicated in the title of each frame. This scaling allows the relatively weak y and z components to be plotted on a similar scale as the x component for clarity. As z increases, the wavefronts curve. This curvature leads to rapid radial phase variations when plotting the field in a plane with a fixed z. To remove this rapid phase variation, the phase (displayed by the colors in the images) are plotted relative to the phase of the x-component of the field: $E_x = |E_x|e^{i\phi_x}$. Thus, the plot of E_x is just its absolute value. This method maps some of the phase variations of E_x observed in its ring structure onto the phase of the plots of E_y and E_z. This artifact is apparent at $z = 0$, but quickly fades for larger z. For these animations we model focusing with $f/(2w) = 1$ ($NA = 0.47$). For larger values of $f/(2w)$, this ratio is similar to the f-number.

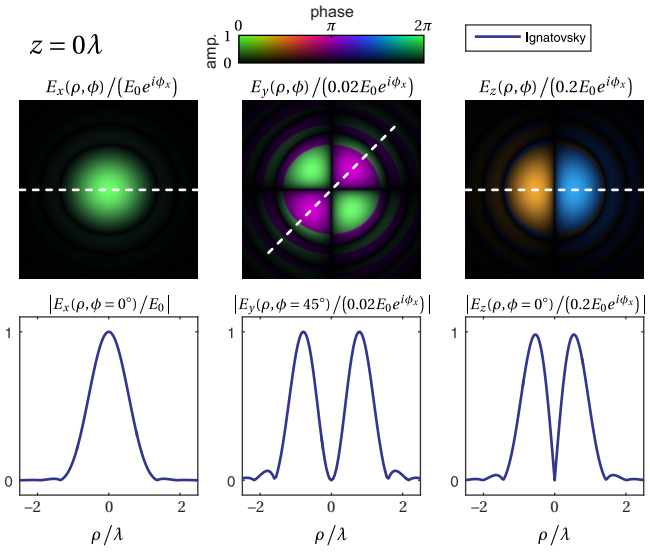

Fig. 5. Animation showing field components for Gaussian beam focused with $f/(2w) = 1$ ($NA = 0.47$) computed with the Ignatovsky model (see Visualization 1). The dashed lines in the upper frames show the locations of line-outs that are plotted beneath. The ρ dimensions on the lower graphs correspond to the ρ dimensions of the square images above. The phase displayed by the colors in the images is relative to the phase of the x-component of the field: $E_x = |E_x|e^{i\phi_x}$. E_0 denotes the maximum value of E_x at $z = 0$.

Figures 6, 7 and 8 show animations of Singh, Davis, and Barton models, respectively. For these figures, the line-out from the Ignatovsky model shown in Fig. 5 is repeated to allow for easy comparison. The models were each fit to the x component of the Ignatovsky result in the focus by adjusting z_0 and E_0. Note that in the Ignatovsky formula, E_0 represents the field amplitude at the center of the focusing mirror, whereas in the other models E_0 represents the field in the center of the focus.

Optics EXPRESS

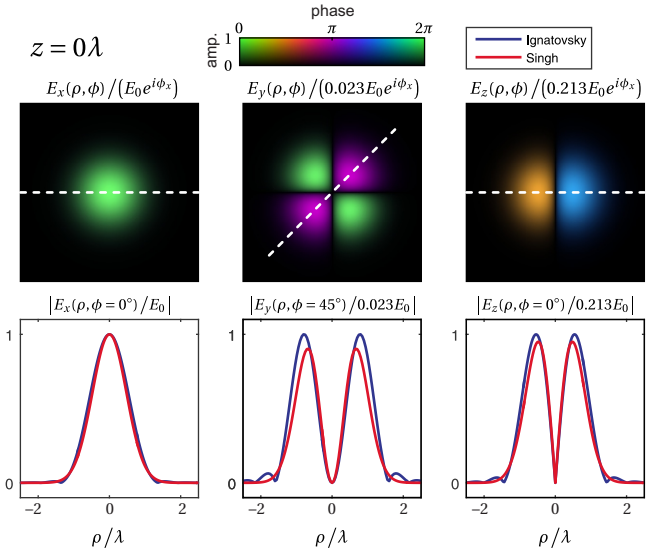

Fig. 6. Animation showing the Singh model for the same parameters used in Fig. 5 (Visualization 2). For comparison, the Ignatovsky result from Fig. 5 is also plotted in the lower frames.

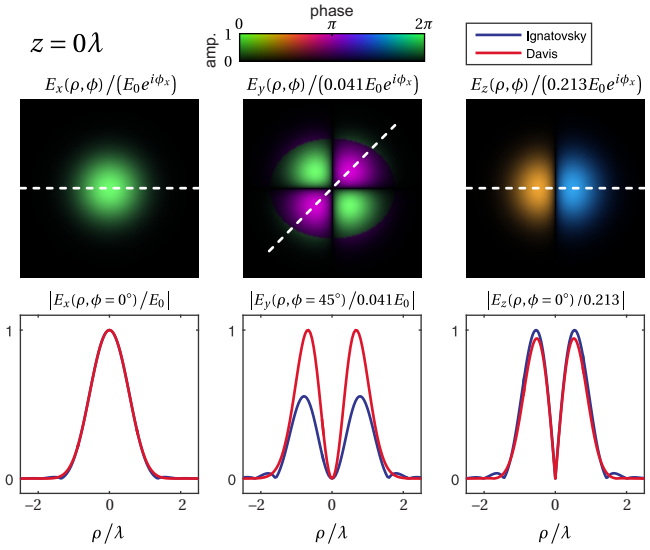

Fig. 7. Animation similar to Fig. 6 using the Davis model (Visualization 3).

Discrepancies between all of the models and Ignatovsky diffraction are apparent. The relatively simple Singh model matches the Ignatovsky result quite well, with only modest differences everywhere and no divergence issues. In the Davis model, the y components of the electric field is off by a factor of two. The Barton model matches the Ignatovsky result slightly better than the Singh or Davis model in the focus near $z = 0$. However, both the Davis and Barton models are seen to wildly diverge in the far field. In contrast, the Singh model tracks the field reasonably well both inside and outside of the focus.

For this comparison we have chosen a relatively wide-angle focusing geometry (~ f/1) to

Optics EXPRESS

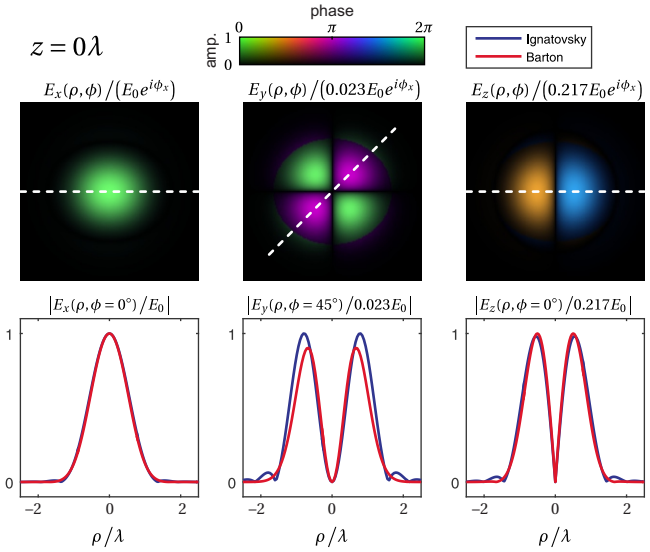

Fig. 8. Animation similar to Fig. 6 using the Barton model (Visualization 4).

emphasize the differences between the models. For the more common cases, where the focusing is not so harsh, the symmetrized models agree quite well near the focus, and the divergence issue for the Barton model is postponed until larger z. The relatively good agreement between the Singh model and the Ignatovsky result suggests particular utility. The Singh model provides a simple analytic form with no divergence issues and good accuracy, at least for the looser focal geometries commonly used in experiments.

8. Other models

We comment on several related vector models of a laser focus: Refs. [6, 8, 11, 18]. These models are somewhat akin to the work of Ignatovsky in that their formulas involve one-dimensional integrals similar to (16). Thus, there is essentially no computational advantage to using this type of model over the Ignatovsky result. Of the models mentioned, that of Quesnel and Mora [18] obeys the symmetry of (25) and has the best chance of agreement with Ignatovsky diffraction for a uniformly polarized Gaussian beam incident on a parabolic mirror. Sepke et al. employ the same symmetrized model but with the options of super Gaussian and annular focal shapes. The vector fields for the Quesnel model are given by

$$\mathbf{E}_{\text{Quesnel}} = E_0 e^{-i\omega t}\left[\hat{x}\left(\tilde{I}_1 + \frac{x^2-y^2}{k\rho^3}\tilde{I}_2 + \frac{y^2}{\rho^2}\tilde{I}_3\right) + \hat{y}\frac{xy}{\rho^2}\left(\frac{2}{k\rho}\tilde{I}_2 - \tilde{I}_3\right) - i\hat{z}\frac{x}{\rho}\tilde{I}_4\right] \tag{29}$$

$$\mathbf{B}_{\text{Quesnel}} = \frac{E_0}{c} e^{-i\omega t}\left[\hat{x}\frac{xy}{\rho^2}\left(\frac{2}{k\rho}\tilde{I}_2 - \tilde{I}_3\right) + \hat{y}\left(\tilde{I}_1 + \frac{x^2-y^2}{k\rho^3}\tilde{I}_2 + \frac{x^2}{\rho^2}\tilde{I}_3\right) - i\hat{z}\frac{y}{\rho}\tilde{I}_4\right] \tag{30}$$

where

$$\begin{aligned}
\tilde{I}_1 &= a\int_0^1 e^{-ab^2}\left(1+\sqrt{1-b^2}\right)e^{ikz\sqrt{1-b^2}}J_0(k\rho b)\,b\,db \\
\tilde{I}_2 &= a\int_0^1 e^{-ab^2}\frac{1}{\sqrt{1-b^2}}e^{ikz\sqrt{1-b^2}}J_1(k\rho b)\,b^2\,db \\
\tilde{I}_3 &= a\int_0^1 e^{-ab^2}\frac{1}{\sqrt{1-b^2}}e^{ikz\sqrt{1-b^2}}J_0(k\rho b)\,b^3\,db
\end{aligned} \tag{31}$$

Optics EXPRESS

$$\tilde{I}_4 = a \int_0^1 e^{-ab^2} \left(1 + \frac{1}{\sqrt{1-b^2}}\right) e^{ikz\sqrt{1-b^2}} J_1(k\rho b)\, b^2 db \tag{32}$$

with $a = (kw_0/2)^2$.

Figure 9 compares the Quesnel model to Ignatovsky diffraction. Note that the y-component of the field differs from the Ignatovsky by approximately a factor of two near $z = 0$, but approaches the Ignatovsky result at large z. This does not imply that the Quesnel model disrespects Maxwell's equations, only that it is associated with a different field than is created by a uniformly-polarized Gaussian beam reflecting on-axis from a paraboloid. Owing to the unique spatial field distribution, the y-component shows some high frequency oscillations with z in the amplitude in the transition for the focal region to the far field. Quesnel and Mora also offer an analytic approximation to their formula [18], which is not analyzed here.

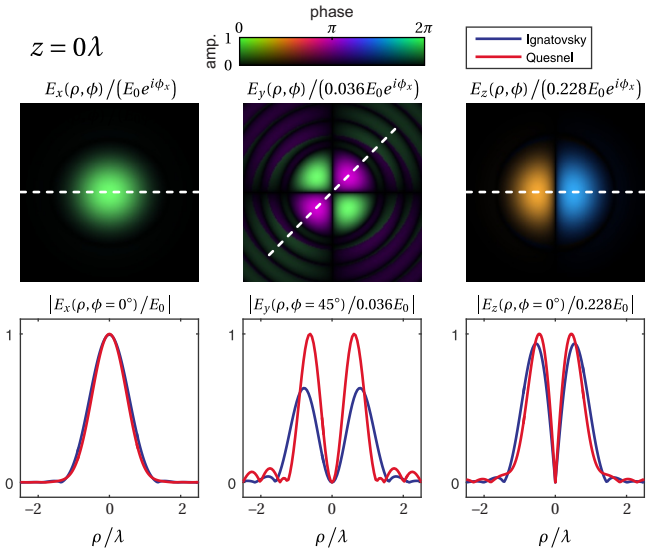

Fig. 9. Animation similar to Fig. 6 using the Quesnel model (Visualization 5).

9. Discussion

In this article we considered a variety of vector laser-focus models in wide use and compared them to the exact result for a collimated linearly-polarized beam focused by an on-axis parabolic mirror. Of the analytic models, we endorse the Singh model as a convenient analytic approximation that closely mimics Ignatovsky's integral formulas down to f/2 focusing. The remarkably good agreement for this looser focusing geometry is shown in Fig. 10. At this level of focusing, there is little benefit to using the refinements in the Barton model, even in the vicinity of the focus, and the Singh model completely avoids divergence issues. If accurate results are required for tighter focusing, it may be best to employ the more computationally-intensive Ignatovsky result directly. Informal benchmarks indicate that using an analytic model such as the Singh formulas is several thousand times faster than evaluating the full Ignatovsky integral.

A common stumbling block in many of the models is that they start from an *assumed* field distribution in the focal region and develop vector fields, consistent with Maxwell's equations, in the surrounding region. However, no experimenter directly controls the field in the focus, and the ability to directly measure vector components of the fields in an intense focus is limited. Instead, experimenters typically diagnose and manipulate their incident beam at the focusing optic.

Optics EXPRESS

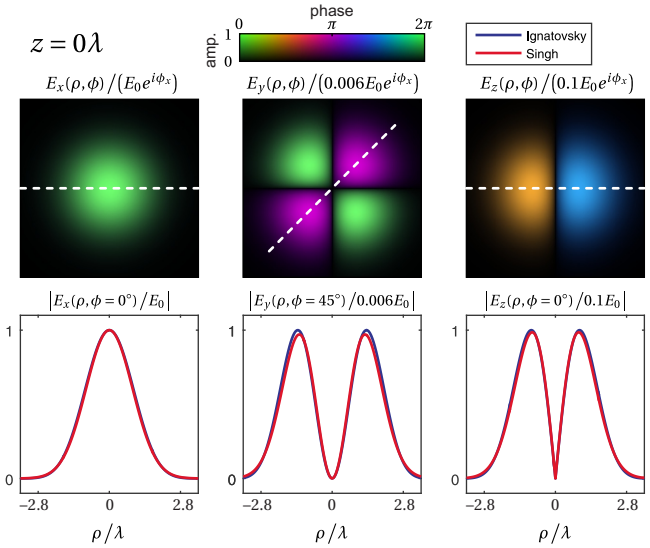

Fig. 10. Animation of the Singh model similar to Fig. 6 using $f/(2w) = 2$ (Visualization 6).

In principle, one could use approaches such as the Quesnel model for the purpose of calculating the field distribution required at a focusing optic to produce a desired field distribution at the focus. A regular profile in the focus tends to correspond to a more complicated distribution outside of the focus, and vice versa, as evidenced by Figs. 2 and 4.

An additional purpose of this article is to draw the attention, especially among the high-intensity community, to the Ignatovsky approach to vector diffraction. The Ignatovsky formula relies on an experimentally relevant boundary condition, and obeys Maxwell's equations exactly everywhere in the beam [46,47]. It is applicable as long as the focusing mirror resides effectively at infinity, which is almost always well fulfilled experimentally (see Appendix A). The work of Ignatovsky is perhaps under-appreciated since it was published in an obscure journal, *Transactions of the Optical Institute of Petrograd*, which resides in the collections of the library of Vavilov State Optical Institute in St. Petersburg, and has not been translated from the original Russian. In 1942, Ignatovsky and his wife were executed by the Soviets on dubious charges of espionage. His sad tale is related in *The Gulag Archipelago* by literary Nobel laureate Aleksandr Solzhenitsyn. Ignatovsky was "rehabilitated" posthumously in 1955 [53].

We presented a self-contained streamlined derivation of Ignatovsky diffraction for a uniformly polarized collimated beam incident on a parabolic mirror. Some authors have referred to Ignatovsky's work as an application of "Debye diffraction" for the fact that it involves convergence of a spherical wave and makes use of the Debye limit of Green's theorem, referred to as the Debye solution [46,47]. However, Ignatovsky deserves considerable credit for being the first to write down the relevant Maxwell-respecting vector fields set up by an experimentally relevant boundary condition, namely a collimated uniformly polarized beam incident on a mirror or lens. Ignatovsky correctly determined the distinct apodizing functions for each of the vector field components before computing their diffracted forms in the vicinity of a focus. We advocate using the term "Ignatovsky vector" to refer to $\hat{\mathbf{p}}^{(E)}$ or $\hat{\mathbf{p}}^{(B)}$ in the generic problem of determining the vector field components of a beam acted upon by a focusing optic.

Ignatovsky's result has appeared in microscopy literature a number of times: In 1959, Wolf and Richards [30,31] produced the first numeric calculations of the vector fields in the focus arising from a plane wave apertured by a finite-diameter lens using the Ignatovsky formula. Sheppard

Optics EXPRESS

et al. [33] examined the problem of vector diffraction by a lens and by a parabolic mirror in 1977, starting from the Stratton-Chu diffraction formula [42]. The analysis for a parabola was repeated by Barakat with a central obscuration [34, 35]. Varga and Török [36] revisited the parabolic-mirror derivation using a different initial field distribution, insisting that reflection from the mirror produces a different vector field than determined by other authors and ourselves. In 2001, Lieb and Meixner [37] made extensive comparisons between the fields produced by a parabolic mirror and by an objective lens. They also explored focusing of an axially polarized field distribution.

A. Recovery of the field at the mirror

In this appendix, we demonstrate that Ignatovsky field expressions evaluated at the mirror surface recovers the incident field. With (1) installed for z, after some manipulation, (15) may be expressed as

$$\mathbf{E}_{\text{mirror}} = -i\frac{ke^{i\left(-\frac{k\rho^2}{4f}-\omega t\right)}}{2\pi f}\int_{-\infty}^{\infty}\int_{-\infty}^{\infty}\frac{dx'dy'}{1+\frac{\rho'^2}{4f^2}}E_{\text{env}}\left(x',y'\right)\hat{\mathbf{p}}^{(E)}\left(x',y'\right)e^{i\frac{k}{2f}\frac{(x'-x)^2+(y'-y)^2}{1+\frac{\rho'^2}{4f^2}}} \tag{33}$$

The integrand is highly oscillatory except in the neighborhood $x' = x$ and $y' = y$, which solely contributes to the integral. Within this neighborhood, the functions $E_{\text{env}}\left(x',y'\right)$ and $\hat{\mathbf{p}}^{(E)}\left(x',y'\right)$, as well as the function $1+\frac{\rho'^2}{4f^2}$, are all slowly varying (by assumption). We may therefore install unprimed variables into each of these. (33) then becomes

$$\mathbf{E}_{\text{mirror}} \to e^{i\left(-\frac{k\rho^2}{4f}-\omega t\right)}E_{\text{env}}\left(x,y\right)\hat{\mathbf{p}}^{(E)}\left(x,y\right)\left[\frac{-ik}{2\pi f\left(1+\frac{\rho^2}{4f^2}\right)}\int_{-\infty}^{\infty}\int_{-\infty}^{\infty}dx'dy'e^{i\frac{k}{2f}\frac{(x'-x)^2+(y'-y)^2}{\left(1+\frac{\rho^2}{4f^2}\right)}}\right] \tag{34}$$

After integration [54], the factor in square brackets works out to be identically one, and (6) is recovered as anticipated. Numerical computation of (33) is in agreement.

A comment is in order regarding the size of the region surrounding $x' = x$ and $y' = y$, over which $E_{\text{env}}\left(x',y'\right)$ and the other functions in (33) are assumed not to vary. The dimension of the neighborhood is characterized by $(x'-x)^2+(y'-y)^2 \sim \lambda f$. For simplicity, we may write

$$\Delta\theta \sim \sqrt{\lambda/f} \tag{35}$$

where $\Delta\theta = \sqrt{\Delta x^2+\Delta y^2}/f$ and Δx, and Δy are lateral displacements in the incident beam from $x' = x$ and $y' = y$ over which $E_{\text{env}}\left(x',y'\right)$, $\hat{\mathbf{p}}^{(E)}\left(x',y'\right)$, and $1+\frac{\rho'^2}{4f^2}$ should remain essentially constant.

The angular extent of acceptable variations, according to (35), shrinks with increasing mirror focal length f. As an example, if $f = 10$ cm and $\lambda = 0.8$ μm, then the field at the mirror should vary only over angular displacements well exceeding $\Delta\theta \sim 3$ mrad, which corresponds to a lateral displacement of $\Delta x, \Delta y \sim 0.3$ mm at the mirror. For a typical beam, which may be centimeters across, this condition is easily fulfilled. While the Ignatovsky formulas are exact solutions to Maxwell's equations, they correspond to an initial field distribution defined on an ideal mirror surface situated at infinity. The use of the Debye limit means that the solution is approximate to the extent that the mirror is positioned at a finite distance.

Funding

Air Force Office for Scientific Research (FA9550-14-1-0345, high-field laser-electron scattering).

Optics EXPRESS

Acknowledgment

This support does not constitute an express or implied endorsement on the part of the Government.